Mechanisms of Friction Reduction in Longitudinal Ultrasonic Surface Haptic Devices with Non-Collinear Vibrations and Finger Displacement

Diana Angelica Torres[1], Eric Vezzoli[2], Betty Lemaire-Semail[1], *Member, IEEE,* Michael Adams[3], *Member, IEEE,* Christophe Giraud-Audine[1], *Member, IEEE,* Frederic Giraud[1], *Member, IEEE* and Michel Amberg [1]

***Abstract*— Friction reduction using ultrasonic longitudinal surface vibration can modify the user perception of the touched surface and induce the perception of textured materials. In the current paper, the mechanisms of friction reduction using longitudinal vibration are analyzed at different finger exploration velocities and directions over a plate. The development of a non-Coulombic adhesion theory based on experimental results is evaluated as a possible explanation for friction reduction with vibrations that are non-collinear with the finger displacement. Comparison with experimental data shows that the model adequately describes the reduction in friction, although it is less accurate for low finger velocities and depends on motion direction.**

Index terms – Surface Haptics, Ultrasonic, Longitudinal, contact mechanics, human skin, occlusion, tribology

I. Introduction

As a result of the development of surface haptic technology, there is a growing demand to develop effective solutions to recreate tactile sensations on flat surfaces such as a glass screen. There are different approaches that are applied to these flat interfaces in order to simulate friction modulation of the fingertip such that it reproduces the vibrational spectra of a sliding finger pad on a real texture [1]. Ultrasonic vibration is one of the leading tactile feedback technologies based on friction modulation that are being developed and coupled with capacitive touch screens. This technology involves ultrasonic vibration to reduce the friction between the contacting finger pad and the display. The aim of the current paper is to explore possible mechanisms that could contribute to this reduction in friction for in-plane longitudinal wave devices, in order to optimize their design and utilization.

Friction reduction by ultrasonic vibration has been largely explored for normal vibration modes [2]–[7]. However, the interaction mechanism through which the friction is reduced is seldom explored, with a few studies including [8]–[10]. For instance, the effect of the exploration direction on longitudinal modes with regards to the wave propagation is one of the subjects that needs a deeper assessment. Thus far, we have relied on the semi-Coulombic, first order 'Bed of Springs' skin model to explain the phenomenon of friction reduction in longitudinal modes [9]. While this model has proven sufficient in one dimension of exploration (along the wave vibration) [10], it is not equipped to detail the change in the dynamic friction coefficient when the finger is sliding over the plate in two dimensions and when there is an angle between vibration axis of the plate and the finger displacement (producing a two dimensional relative motion between the finger pad and the surface). Therefore, analyzing the mechanical phenomena associated with tactile exploration becomes an important task in the creation of a non-Coulombic contact model in two dimensions.

For a longitudinal ultrasonic surface haptic device, the friction modulation that is experienced could be explained by a few simultaneous effects. Friction is the result of the energy dissipated per unit sliding distance in a sub-surface region of the order of 100 nm (interfacial mechanism) or in much deeper regions (deformation mechanism). In the case of skin, it has been shown that the friction is dominated by the interfacial mechanism [11] for which the frictional force is given by the product of the interfacial shear strength and the contact area; this is known as the adhesion mechanism since this shear strength depends on the intermittent formation and rupture of intermolecular bonds such as the ones produced by the van der Waals forces. In the dry state, skin exhibits glassy behaviour and the shear strength is increased gradually with increasing sliding velocity. However, in a persistent contact with an impermeable surface such as glass, a finger pad becomes plasticized by occlusion of the secreted moisture in the sweat such that there is a transition to the rubbery state, which corresponds to the experimental conditions applied in the current work. Generally, the friction as the function of velocity for a rubber sliding on a rough track shows two peaks. One occurs at high sliding velocities and it has been mainly attributed to a viscoelastic contribution and the other, occurring in general at much lower velocities, that correspond to those studied here, which is considered attributable to the adhesion mechanism [12]. The energy dissipation involves the stochastic pinning and depinning of surface polymeric molecules to the counter surface by a stress aided thermally activated process that depends on the surface exploration velocity [11], [13], [14]. At low velocities, there is sufficient time for the molecules to stretch within the critical depinning time. As the velocity increases, the molecular extension increases and, hence, so does the frictional force. However, at higher velocities, the rate of breakage of bonds is greater than their formation, which causes the friction to decrease with increasing velocity. Additionally, if a finger pad behaves like an elastomer, the strength of adhesion generally increases with the time of contact, due to slow molecular

rearrangements that occur at the interface and increase the bond strength.

The real contact area is also an important factor which affects the dynamic friction at different exploration speeds. Assuming constant ridge contact, a Herzian model would result in the evolution of the contact area in the fully occluded state increasing with the normal force to a power $m = 2/3$. However, in reality the contact corresponding to a finger pad and a plate is not Herzian. Consequently, the evolution of the contact area is a complex mechanism that depends on many factors such as the loading [15], the geometry of the finger and ridges [16], the dwell time of the contact [17], [18], the onset of occlusion [13], [17] and the contact deformation due to the velocity and direction of exploration [16].

Therefore, in summary, we could conclude that the friction reduction due to longitudinal vibration cannot be explained by the variation in shear strength because of an augmented relative velocity of the finger against the plate and a reduction in the real contact area.

In the current paper we propose to produce an interaction model able to explain the reduction of friction in the case of a longitudinal wave surface device, using the principle of variation of friction as a function of speed, which involves fitting to the experimental data.

The paper is organized as follows: section *II* briefly explains the effect of exploration speed on the shear strength and contact area in sliding finger contacts. In section *III,* we propose an experiment to measure the change in friction at different speeds for a finger pad without vibration. The measurements are fitted to the model obtained in section *II*. In section *IV*, a series of measurements is made to obtain the mean friction reduction at different speeds and vibration amplitudes, in two different exploration directions. In section *V*, simulations aim to describe the 2-dimensional relative velocities and relative trajectories of the finger against the plate when it is vibrating. The empirical model fitted in section *III* is then used to evaluate whether the friction reduction with a longitudinal ultrasonic vibration can be explained by the changes in the relative velocity of the finger during exploration due to the vibration of the plate. A discussion is presented in section *VI* and conclusions in section *VII*.

II. Friction Variation on a Finger Pad Due to Sliding Velocity

A. Time-constrained shear strength

The sliding velocity range that is most relevant to tactile exploration is about 10–200 mm/s [13]. Within this range, it is possible to find a dynamic friction peak related to adhesion [12]. Provided that a finger pad is sufficiently moist, particularly due to occlusion of moisture secreted from the sweat pores in the finger print ridges, it has been shown [11] that the friction may be described by molecular theories that have been developed for elastomers [14], [19].

The model developed for describing the dependence of dynamic friction on sliding velocity was extended to account for the viscous retardation in [14]. An expression for the equilibrium value of the coefficient of friction, μ_E, was derived and found to be consistent with data measured for the finger pad [11]. In this latter work, the expression was written as in (1).

$$\mu_E = 2\mu^+(q+1)\left\{\frac{V^*\left[1-e^{-1/V^*}\right]-e^{-1/V^*}}{1+q-e^{-1/V^*}}\right\} \qquad (1)$$

The parameter q is a time constant, such that $q = \tau_0/\tau_p$, where τ_0 is the mean lifetime of a pinned polymer chain when the finger is static and τ_p is the lifetime of the pinned chain when the finger is sliding at a velocity V. The velocity ratio corresponds to $V^* = V/V_0$ where V_0 represents the critical velocity at which the stress-aided depinning becomes significant.

The friction coefficient μ^+ corresponds to the maximum value of the friction coefficient μ with respect to the sliding velocity and normal force F_n (i.e. when a maximum number of linking chains are attached over a unit area). All parameters are deduced assuming a standard room temperature.

B. Dwell time, contact area and friction

As mentioned in section I-A, the friction coefficient μ^+ is dependent on the available number of pinned chains per unit area. This is not a constant value. In reality, the availability of such chains is dependent on the real contact area of the fingerprint ridges $A_{junct}(t)$, which, in the case of smooth, impermeable surfaces such as glass, increases very slowly and is a function of moisture and dwell time.

In [17], this temporal evolution of the contact area against glass is described by a first order kinetics equation, where A_0 and A_∞ correspond to A_{junct} at $t = 0$ and $t \to \infty$, respectively and λ is a characteristic time constant (2).

$$A_{junct}(t) = A_\infty + (A_0 - A_\infty)e^{-\left(\frac{t}{\lambda}\right)} \qquad (2)$$

In practice, it is difficult to produce ranges for these values, since there is a very large variability between the different studies on different subjects and materials [17]. Additionally, (2) does not account for the deformation at the contact area between the finger and a flat surface during the onset of tangential sliding movements in the different directions (proximal, distal, radial and ulnar), which vary by different amounts at different values of normal force and tangential speeds [16]. According to this last study, the contact area was more or less inversely proportional to velocity V, and more or less symmetrical in the radial-ulnar direction.

C. Friction function approximation

Considering the various effects that influence the velocity dependent friction function of a finger pad against an impermeable, hard and smooth surface such as glass, it is difficult to produce a completely analytical model. We propose therefore a simplified adaptation of (1), modifying $\mu^+$to be $\mu(V)$, a friction factor dependent on speed, described by a second order kinetics equation (4).

$$\mu_E = 2\mu^*(q+1)\left\{\frac{V^*\left[1-e^{-1/V^*}\right]-e^{-1/V^*}}{1+q-e^{-1/V^*}}\right\} \quad (3)$$

$$\mu^*(V) = \mu_{t\to 0} + (\mu_{t\to\infty} - \mu_{t\to 0})e^{-\left(\frac{V^2}{k_V}\right)} \quad (4)$$

Therefore, we could find limit values for μ^*, which would account for friction variations dependent on exploration speed, such as junction area increase, stretch increase of the individual linking chains, and gross area deformation, as in (4), with a pinning constant k_V. This model can be fitted to average experimental data, in order to obtain the values $\mu_{t\to\infty}$, $\mu_{t\to 0}$, k_V, together with q and V_0. We assume for these measurements that they are obtained at almost constant normal forces F_n after a period t, which is sufficient for processes such as occlusion to equilibrate.

III. Friction vs. Sliding Velocity Measurements

A. Material

Fig. 1 shows the experimental equipment that includes a longitudinal surface haptic device, built as described in [20]. It is composed of an aluminum plate with dimensions 128 x 30 x 1.94 mm. At the center of the upper and lower surfaces, a matrix of 12 piezoelectric ceramics of dimensions 5 x 9 x 0.3 mm are adhered to the aluminum. The surface of the haptic device is considered to be optically smooth and is coated with a damp-proof polymeric material.

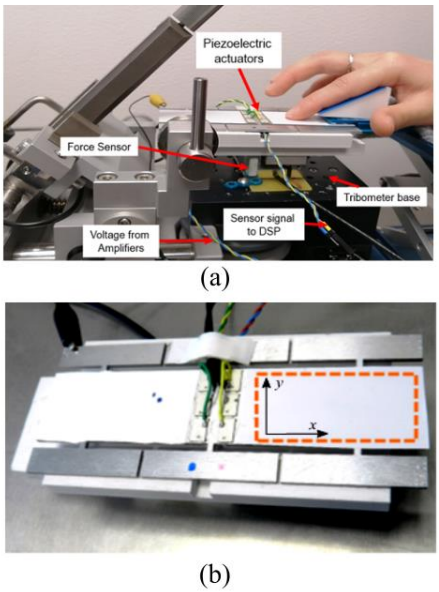

Figure 1. (a) Haptic device with three-axial force sensor and tribometer base. (b) illustration of the x and y directions over the exploration area. During the experiment the tribometer base moves while the finger presses statically.

The deformation induced on the plate is the result of opposite surface tensions induced on both sides of the plate by the piezoelectric ceramics. As explained in [20], it was confirmed through cartography measurements that the lateral motion induced on the surface is primarily along the x axis, with very low comparative residual motion along the y and z axes (< 2%).

The device is positioned on the moving base of a tribometer. Below the device, a three-axis force sensor (GSV-4USB from ME-Meßsysteme) is installed to record the normal and friction forces. A support is installed for the hand and finger, so that they may be properly positioned over the surface of the device.

B. Friction measurement without vibration

In the initial phase of the experiment, a participant is asked to clean and dry his (her) finger, and to position it on the right part of the surface, as shown in fig. 1.

A visual interface allows the participant to maintain an appropriate normal force on the device of about 0.5 N. The base of the tribometer is programmed to perform several reciprocating motions below the static finger, while the information is recovered with the three-axial force sensor.

After the finger is positioned on the plate, eight reciprocating motions were applied before beginning the data acquisition. The coefficient of friction was calculated by dividing the force measurement on the x axis by the force in the z axis, for over 10 periods. To change the direction of the exploration, the device was repositioned on the tribometer base.

Friction measurements were obtained in the range of 20 to 140 mm/s in increments of 20 mm/s. The mean friction at each velocity was recorded. Measurements were then repeated for a group of eight participants aged between 18 and 60 years. All participants gave informed consent. The investigation conformed to the principles of the Declaration of Helsinki and experiments were performed in accordance with relevant guidelines and regulations.

The mean values and standard deviation of the friction measurements without vibration as a function of the sliding velocity for the eight participants are shown in fig. 2. These data is fitted to eq. (3) and (4). As expected, the peak friction value corresponds to about 20 to 60 mm/s, followed by a steady reduction up until 140 mm/s. From 120 mm/s, some participants show an increase of the dynamic friction.

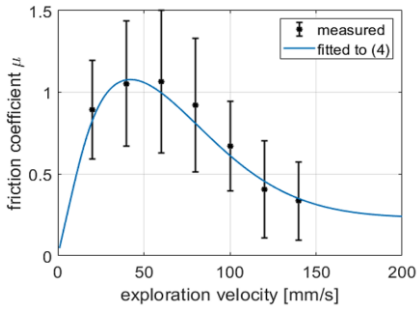

Figure 2. Mean and standard deviation of friction coefficient measurement with no vibration at several velocities for eight paticipants (black) vs. fitted model calculated using Eq. (3)

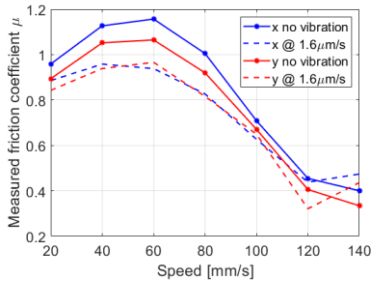

Figure 3. Mean friction measurements with and without vibration at different finger speeds for the x and y exploration direction with Fn=0.5N. To change the direction the device is repositioned on the base.

The mean values of friction are fitted to (3), as can be seen in fig. 2, with $\mu_{t\to\infty} = 1.86$, $\mu_{t\to 0} = 0.156$, $k_V = 0.0048\ \mathrm{m^2/s^2}$, $q = 0.0177$ and $V_0 = 68\ \mathrm{mm/s}$.

C. Friction measurement with vibration

Using the procedure described in section *III.B*, the friction measurements were made with all participants at the same velocities as the previous experiment. In this case, a longitudinal closed loop vibration of about 58 kHz at six different vibration amplitudes of 0, 0.8, 1, 1.2, 1.4 and 1.6 $\mu\mathrm{m_{p-p}}$ is imposed on the device. Higher amplitudes produce more reduction, as observed in [10].

The measurements were done as the finger explores along the *x* axis that corresponds to the long surface, which is the direction of propagation of the longitudinal wave. This was repeated in the orthogonal *y* direction. The finger moves always in the radial-ulnar direction.

Fig. 3 shows the mean values of the coefficients of friction as a function of the sliding velocity along the *x* and the *y* axes without vibration, and with a vibration amplitude of 1.6 $\mu\mathrm{m_{p-p}}$. The mean friction in the *x* direction without vibration appears slightly greater than that in the *y* direction but probably this is within the experimental uncertainty. Nevertheless, we observe that the reduction is similar in both cases. It is more important at lower velocities, below about 90 mm/s.

IV. Finger Pad Relative Motion and Friction

A. Spring slider model with non-Coulombic dynamic friction

When the skin slides over the flat surface of the haptic device, it experiences a frictional force that depends on the speed of exploration. When a longitudinal vibration is imposed on the device, the relative speed of the finger pad over the surface is modified. Consequently, the stratum corneum (sc) is expected to be deformed and then to slide over the surface. To calculate the reactive force produced from this interaction, a simplified polar spring-slider model is proposed. It visualizes the skin as a damped spring that is deformable in any direction over the *xy* plane. The interaction can thus be visualized as a state machine with two different states, '*sticking*' and '*sliding*'[9], [10]. When sticking, the deformation of the dampened spring produces a radial force F_r in the direction of the motion, equal to $F_r = K_s r_f + D_s \dot{r}_f$, with r_f representing the radial elongation of the spring K_s, $\dot{r}_f$ is the velocity of this elongation, and the parameters K_s and D_s define the static elasticity and damping of the sc respectively.

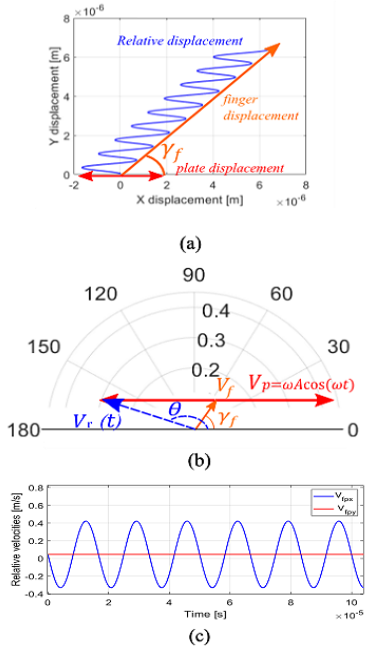

Figure 4. Motion of the finger with and without ultrasonic vibration. (a) Displacement of the finger relative to the plate in a cartesian coordinate system. The trajectory of the finger (orange) and the plate motion (red) are represented for the theoretical example: $\gamma_f(t) = \pi/3$, $V_f(t) = 60\mathrm{mm/s}$, $A = 1\ \mu\mathrm{m_{p-p}}$ and $2\pi\omega = 60$ kHz. The *xy* plane corresponds to the surface of one facet of the haptic device. (b) Representation of the velocities in the polar coordinate system. The velocity of the finger (orange) is added to the plate velocity (red), which depends on time, producing $V_r(t)$ and angle θ(t). (c) Relative velocities V_{fpx} and V_{fpy} in function of time

The 'sticking' state is induced only when $\dot{r}_f = 0$ and corresponds to a no-slip boundary condition. During this state, the skin remains stuck to the surface of the plate. The relative motion of the skin against the plate stretches the sc until the absolute value of the radial force is larger than the static friction coefficient multiplied by the pressing force F_n, i.e. $|F_r| > \mu_s F_n$. Subsequently, the skin is '*sliding*, and F_r will be dependent on F_n and the dynamic friction coefficient.

In this paper, it is assumed that, unless the finger slides along the direction of the longitudinal wave propagation, it remains in the sliding state.

B. Relative radial velocity and trajectory: Example

To calculate the relative velocity between the finger and the plate, V_{fp} , during active exploration over the *xy* plane, we assume that the finger is moving with a velocity of magnitude $V_f(t)$ and angle $\gamma_f(t)$, as shown in fig. 4. The plate is simultaneously vibrating along the *x* axis following a motion described by $w = (A/2)\sin\omega t$ and therefore a speed of $V_p = \dot{w} = \omega\,(A/2)\cos(\omega t)$, with $(A/2)$ being the vibration amplitude (typically within the range of a few micrometers) and ω being the vibration angular frequency. The relative velocity of the finger viewed from the vibrating plate V_{fp} is described by (5).

$$V_{fpx}(t) = V_f(t)\cos\big(\gamma_f(t)\big) - \omega\,(A/2)\cos(\omega t) \qquad (5)$$
$$V_{fpy}(t) = V_f(t)\sin\big(\gamma_f(t)\big)$$

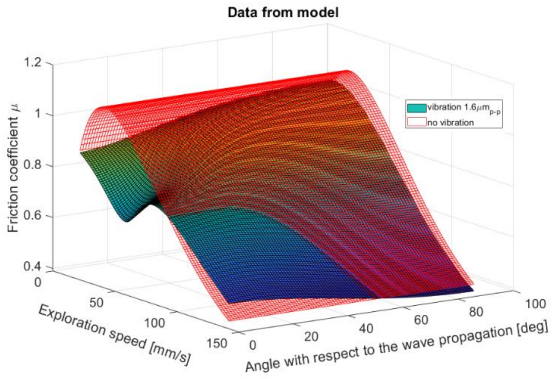

Figure 5. Simulation of the relative velocity dependent dynamic friction from the model described in (4), with the velocity $V^* = V_r$, with V_r calculated for every finger exploration angle γ_f from 0° to 90° as described in (5).

From the velocities described in the Cartesian coordinate system in (5), it is possible to calculate the relative velocity V_{fp} in the polar coordinates, which we can term $V_r(t)$, the relative angle in the polar coordinates, which we term $\theta(t)$ and angle variation $\dot{\theta}$.

We may therefore deduce that whenever $A \neq 0$, the mean value of the finger velocity over a time period $\bar{V}_f$ is smaller than the mean magnitude of the relative velocity $|\bar{V}_r|$. This velocity variation will produce a variation in the dynamic friction coefficient according to (3)-(4).

Fig. 5 represents the result of this calculation for $V_f(t)$ ranging between 0-150 mm/s and γ_f from 1° to 90°. For this example, we evaluate the cases $A = 0\mu m_{p-p}$ (red) vs. $A = 1.6\ \mu m_{p-p}$(blue) at $\omega/2\pi = 58$ kHz.

It can be noted that as the angle γ_f approaches the value $\gamma_f = k\pi$ (with $k = 0,1,2,3,\ldots$), the friction reduction due to the vibration becomes more significant at lower V_f. It is important to consider, however, that at these low angles, the model might be less accurate than at higher angles, given the assumption that the finger remains in the sliding state. In particular, we do not find the same behavior than the measured one, depicted in fig.3, for the x direction (dashed blue line). Indeed, in general, it is possible that some partial sticking and torsion might take place when the displacement in y is small, producing a difference between the measured friction and the model predictions. In order to test the accuracy of the proposed model without the mentioned bias for lower values of V_{fpy}, subsection *IV C* evaluates the friction model against measurements in the limit case $\gamma_f(t) = \pm\pi/2$.

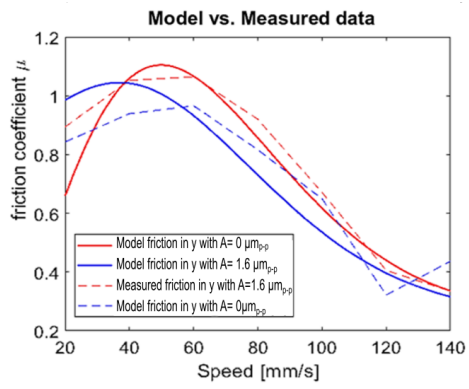

Figure 6. Measured and calculated friction coefficients with and without vibration as a function of the exploration speed with the finger exploring at $\gamma_f = (\pm\pi)/2$ and a vibration amplitude of 1.6μm_{p-p}

C. Friction Reduction Evaluation for $\gamma_f(t) = \pm\pi/2$

To compare the theoretical values against the actual friction reduction, we consider the limit case $\gamma_f(t) = \pm\pi/2$. Friction measurements were taken at different exploration velocities between 0 and 140 mm/s in the case where there is no vibration, and then when A=1.6 μm_{p-p}.

The dynamic friction is calculated from the model at every sampling point. The simulation results are compared with the measurements. The results are plotted in fig. 6.

To evaluate the quality of the model, we calculate the mean relative error for the set of k measurements in the velocity range as: $err\mu\% = mean\left(\frac{|\mu_k - \mu_{k_{est}}|}{\mu_k}\right)$. The error for the model without vibration is 5.5%. The error of the model with a vibration of 1.6 μm_{p-p} is of 11.2%.

It can be concluded that, although there is a considerable error in the low velocity range, the overall effect of the vibration on friction is correctly described by the model.

V. Discussion

In this paper, a friction reduction model is proposed based on the relative motion analysis and the dynamic dependence of friction with the exploration velocity. This approach has been introduced to explain the friction reduction observed, even if the finger movement is not colinear with the longitudinal wave direction. Indeed, in that case, the modelling explained in [9], [10] for γ_f=kπ (with k=0,1,2,3,…) is no more relevant, unless taking into consideration partial torsion and partial sticking phenomena which seems to be quite difficult. Moreover, another phenomenon has also to be considered, which is all the more significant that the finger slides (without sticking) on the surface, that is the speed dependency of the friction. Within this "sliding" assumption, the friction will mainly depend on the velocity dependence of the dynamic friction coefficient $\mu_d(V_r(t))$.

The simplified model described in the current work is useful in order to establish key principles that could be useful for formulating models and that are more complete, in future research.

The results plotted in fig. 3 show the friction reduction at a number of velocities in the x and y directions for a given vibration amplitude. It is important to note that, while the friction reduction produced by the ultrasonic longitudinal vibration seems relatively small in comparison to the reduction observed at high velocities, even without vibration, a comparison with classic ultrasonic devices (which use out-of-plane modes) [21] shows that longitudinal modes have the potential to be more energy efficient in terms of the active power required to produce a given friction contrast, and thus a desired sensation.

VI. Conclusion

In the current work, we introduced a mechanical model of the interaction of a finger pad and a surface during active exploration that is applicable to longitudinal mode vibration in the ultrasonic domain. The model allows the friction as a function of the relative sliding velocity due to the longitudinal vibration to be explained, in the case where the exploration does not occur along the direction of the wave propagation.

Comparison with experimental data shows that the model adequately describes the reduction in friction for the sliding speeds that are comparable to active touch, but the model is less accurate at lower velocities and angles. This may be the result of additional mechanisms, which will be the subject of future research.

Acknowledgment

This work has been carried out within the framework of the Mint Project of IRCICA (CNRS Service and Research Unit 3380).

References

[1] M. Wiertlewski, J. Lozada, and V. Hayward, "The Spatial Spectrum of Tangential Skin Displacement Can Encode Tactual Texture," *IEEE Transactions on Robotics*, vol. 27, no. 3, pp. 461–472, Jun. 2011

[2] T. Watanabe and S. Fukui, "A method for controlling tactile sensation of surface roughness using ultrasonic vibration," in *Proceedings of 1995 IEEE International Conference on Robotics and Automation*, May 1995, vol. 1, pp. 1134–1139 vol.1.

[3] M. Biet, F. Giraud, and B. Lemaire-Semail, "Squeeze film effect for the design of an ultrasonic tactile plate," *IEEE Transactions on Ultrasonics, Ferroelectrics and Frequency Control*, vol. 54, no. 12, pp. 2678–2688, Dec. 2007.

[4] Wiertlewski M, Friesen RF, Colgate JE. Partial, "Squeeze film levitation modulates fingertip friction". *Proceedings of the national academy of sciences*. 2016 Aug 16;113(33):9210-5.

[5] F. Giraud, T. Hara, C. Giraud-Audine, M. Amberg, B. Lemaire-Semail, and M. Takasaki, "Evaluation of a friction reduction based haptic surface at high frequency," in *2018 IEEE Haptics Symposium*, San Francisco, CA, Mar. 2018, pp. 210–215.

[6] E. Vezzoli, V. Zlatko, G. Vincenzo, B. Lemaire-Semail, F. Giraud, R. Tomaz, P. Djordje, M. Adams, "Friction Reduction through Ultrasonic Vibration Part 1: Modelling Intermittent Contact," *IEEE Transactions on Haptics (ToH)*, vol. 10, no. 2, pp. 196–207, 2017.

[7] R. F. Friesen, M. Wiertlewski, and J. E. Colgate, "The Role of Damping in Ultrasonic Friction Reduction," in *2016 IEEE Haptics Symposium (HAPTICS)*, Philadelphia, PA, Apr. 2016, pp. 167–172.

[8] H. Xu, M. A. Peshkin, and J. E. Colgate, "UltraShiver: Lateral force feedback on a bare fingertip via ultrasonic oscillation and electroadhesion," in *2018 IEEE Haptics Symposium (HAPTICS)*, Mar. 2018, pp. 198–203.

[9] E. Vezzoli, B. Dzidek, T. Sednaoui, F. Giraud, M. Adams, and B. Lemaire-Semail, "Role of fingerprint mechanics and non-Coulombic friction in ultrasonic devices," in *2015 IEEE World Haptics Conference (WHC)*, Evanston, IL, Jun. 2015, pp. 43–48.

[10] D. A. Torres Guzman, B. Lemaire-Semail, A. Kaci, F. Giraud, and M. Amberg, "Comparison Between Normal and Lateral Vibration on Surface Haptic Devices," in *2019 IEEE World Haptics Conference (WHC)*, Tokyo, Japan, Jul. 2019, pp. 199–204.

[11] S. M. Pasumarty, S. A. Johnson, S. A. Watson, and M. J. Adams, "Friction of the Human Finger Pad: Influence of Moisture, Occlusion and Velocity," *Tribol Lett*, vol. 44, no. 2, pp. 117–137, Nov. 2011.

[12] A. Genovese, F. Carputo, M. Ciavarella, F. Farroni, A. Papangelo, and A. Sakhnevych, "Analysis of Multiscale Theories for Viscoelastic Rubber Friction," in *Proceedings of XXIV AIMETA Conference 2019*, Springer International Publishing, 2020, pp. 1125–1135.

[13] M. J. Adams *et al.*, "Finger pad friction and its role in grip and touch," *Journal of The Royal Society Interface*, vol. 10, no. 80, pp. 20120467–20120467, Dec. 2012.

[14] Y. B. Chernyak and A. I. Leonov, "On the theory of the adhesive friction of elastomers," *Wear*, 108 (1986) 105 - 138.

[15] B. M. Dzidek, M. J. Adams, J. W. Andrews, Z. Zhang, and S. A. Johnson, "Contact mechanics of the human finger pad under compressive loads," *J. R. Soc. Interface.*, vol. 14, no. 127, p. 20160935, Feb. 2017.

[16] B. Delhaye, P. Lefèvre, and J.-L. Thonnard, "Dynamics of fingertip contact during the onset of tangential slip," *J. R. Soc. Interface.*, vol. 11, no. 100, p. 20140698, Nov. 2014.

[17] B. Dzidek, S. Bochereau, S. A. Johnson, V. Hayward, and M. J. Adams, "Why pens have rubbery grips," *Proc Natl Acad Sci USA*, vol. 114, no. 41, pp. 10864–10869, Oct. 2017.

[18] A. J. Tuononen, "Onset of frictional sliding of rubber–glass contact under dry and lubricated conditions," *Sci Rep*, vol. 6, no. 1, p. 27951, Sep. 2016.

[19] A. Schallamach, "A theory of dynamic rubber friction," *Wear*, vol. 6, no. 5, pp. 375–382, Sep. 1963.

[20] D. A. Torres, B. Lemaire-Semail, C. Giraud-Audine, F. Giraud, and M. Amberg, "Design and control of an ultrasonic surface haptic device for longitudinal and transverse mode comparison," *Sensors and Actuators A: Physical*, vol. 331, p. 113019, Nov. 2021.

[21] D. A. Torres Guzman, B. Lemaire-Semail, F. Giraud, C. Giraud-Audine, and M. Amberg, "Energy Analysis of Lateral vs. Normal Vibration Modes for Ultrasonic Surface Haptic Devices," in *Haptics: Science, Technology, Applications*, vol. 12272, I. Nisky, J. Hartcher-O'Brien, M. Wiertlewski, and J. Smeets, Eds. Cham: Springer International Publishing, 2020, pp. 416–424.